ADVANCED ANALYSIS METHOD OF ELECTRIC PROPULSION SYSTEM FOR UAM VEHICLES

Donguk Lee[1], Kwanjung Yee[1]*

[1]Dept. of Aerospace Engineering
Seoul National University, Seoul, 08826, Republic of Korea
oak600p@snu.ac.kr / kjyee@snu.ac.kr

ABSTRACT

This article proposes an advanced analysis method of the electric propulsion system for UAM vehicles. Three modules are constructed to consider the electrical characteristics of electric devices. The motor-analysis module is developed based on the permanent magnet synchronous motor (PMSM)'s control strategies: maximum torque per ampere (MTPA), field weakening (FW), and maximum torque per voltage (MTPV). The inverter-analysis module uses the linear loss model for the power semiconductors. Based on the near-linear discharge model, the battery-analysis module was constructed to consider the voltage drop. In addition, the eVTOL aircraft sizing is performed in two cases depending on the type of analysis method for the electric propulsion system. The comparative study based on the sizing results demonstrates the necessity and the capability of the proposed analysis method for the electric propulsion system.

NOMENCLATURE AND ABBREVIATIONS

$E_{\mathrm{on,off}}$	Turn-on and turn-off energies
f_{S}	Switching frequency
G	Change in the slope of the discharge curve due to current
$I_{\mathrm{d,q}}$	d- and q-axis current
I_{ref}	Reference current which is the on-state current after the commutation
I_s	Current space vector
I_{sm}	Voltage space vector
K	Primary dependency of voltage on the capacity discharged
$L_{\mathrm{d,q}}$	d- and q-axis inductance
M	Modulation index
MTOW	Maximum take-off gross weight
N	Number of battery cell
P	Power
P_{Cu}	Copper loss
P_{Fe}	Iron loss
P_{lc}	Conduction loss
P_{ls}	Switching loss
$P_{\mathrm{no-load}}$	No-load power
P_{p}	Number of pole-pair
Q	Total capacity discharged up to the present instant
R	Internal resistance of the battery cell
R_{ce}	IGBT's differential resistance
R_{F}	Diode's differential resistance
R_{s}	Phase resistance
SP	Specific power
T	Torque
V_0	Open circuit (no load) voltage
V_{ce}	IGBT's threshold voltage
$V_{\mathrm{d,q}}$	d- and q-axis voltage
V_{DC}	DC link voltage
V_{F}	Diode's threshold voltage
V_{ref}	Reference voltage which is the blocking state voltage of the IGBT before the commutation
V_s	Voltage space vector
V_{sm}	Voltage constraint
β	Phase angle
η	Efficiency
λ_0	Stator permanent magnet flux linkage
ω_{b}	Base speed
ω_{e}	Electrical velocity

1. INTRODUCTION

According to the World eVTOL Aircraft Directory [1], more than 300 electric vertical take-off and landing (eVTOL) aircraft for urban air mobility (UAM) have been developed since the release of the Uber Elevate white paper in 2016. Approximately 70% of eVTOL aircraft use a full-electric propulsion system, which draws energy solely from batteries. A full-electric propulsion system has shown not only the reduction of carbon footprints but also enables significant design freedom for various advantageous interactions that were not previously considered in the aircraft design (e.g., distributed propulsion; DP). Therefore, rotorcraft community has been challenged to design the electrified rotorcraft.

However, previous studies [2–9] concerning the eVOTL aircraft design have been somewhat limited to reflect the electrical characteristics since the analysis method for the electric propulsion system has the

Presented at 45th European Rotorcraft Forum, Warsaw, Poland, 17-20 September, 2019

fidelity of a low standard. de Vries et al. [2-4] established a sizing method to incorporate various electric propulsion systems into a single matrix form by using the electric devices' efficiency coefficient as a constant. Finger et al. [5-7] modernized the classical conceptual design method by adding a hybridization factor to the point-performance and mission-performance modules. With this factor, the suggested methodology could cover the various types of electrified propulsion systems—full-electric and hybrid-electric propulsion system—by using the electric devices' efficiency coefficient as a constant. Lukaczyk et al. [8] developed a generic conceptual design tool by integrating multidisciplinary analysis modules: aerodynamics, structures, stability&control, propulsion, and etc. The suggested tool implements the electric propulsion system analysis module using the motor efficiency map without circuit analysis. Malpica et al. [9] conducted a study of the handling qualities of quadrotor designs for UAM application using the NDARC, which uses a motor-analysis module focused on the BLDC motor type.

In short, most existing analysis methods for the electric propulsion system did not consider electric circuits for electric devices but used specific constant or datasheets. The efficiency of electric devices actually changes according to the current and voltage required to perform the mission, and a voltage drop also occurs according to the total capacity discharged. Since these features affect the fidelity of analysis and the reliability of the design, there is a need to reflect them in the eVTOL aircraft analysis and design. In addition, instead of the BLDC type, a permanent magnet synchronous motor (PMSM)—a representative AC motor type—should be considered for the high output of power and efficiency required to design UAM vehicles.

Thus, this study aimed to suggest an advanced analysis method of the electric propulsion system for UAM vehicles that can consider the electric characteristics of electric devices—motor, inverter, and battery. First, the motor-analysis module was developed based on PMSM's control strategies—maximum torque per ampere (MTPA), field weakening (FW), and maximum torque per voltage (MTPV). The inverter-analysis module was created using the linear loss model for the power semiconductors. The battery-analysis module was constructed to consider the voltage drop, where the near-linear discharge model was used.

This paper is organized as follows: First, Section II describes three modules for the motor-analysis, inverter-analysis, and battery-analysis. Section III outlines the conceptual design methodology with the proposed analysis method. Section IV discusses a comparative study between the proposed analysis method and previous counterpart. Finally, Section VI provides the summary of this study.

2. ANALYSIS MODULES FOR THE ELECTRIC PROPULSION SYSTEM

2.1. Motor Analysis

The mathematical modeling of the PMSM uses an equivalent circiut model based on the d- and q-coordinates, as shown in Fig. 1.

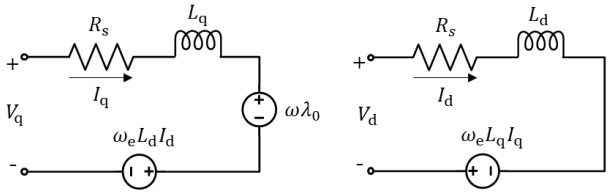

(a) q-axis (b) d-axis

Figure 1 Equivalent circuit model of the PMSM

To consider the rated power limitation, PMSM's armature current I_s and terminal voltage V_s have constraints as follows [Eq.(1), (2)]:

(1) $I_s = \sqrt{I_d^2 + I_q^2} \leq I_{sm}$

(2) $V_s = \sqrt{V_d^2 + V_q^2} = \omega_s \sqrt{\lambda_d^2 + \lambda_q^2} \leq V_{sm}$

In this study, three control strategies [10] that can efficiently operate PMSM under these limited operating conditions are used as bellows:

- *MTPA control*: MTPA control is a concept to find the current operating point that can output the maximum torque under the constant stator current amplitude.
- *FW control*: FW control is a concept to enable higher motor speeds by reducing the back-EMF generated by the motor.
- *MTPV control:* MTPV control is a concept to produce the maximum torque under the voltage-limit condition, where the current-limit condition is not considered.

Figure 2 shows the optimal current vector trajectory based on the three control strategies.

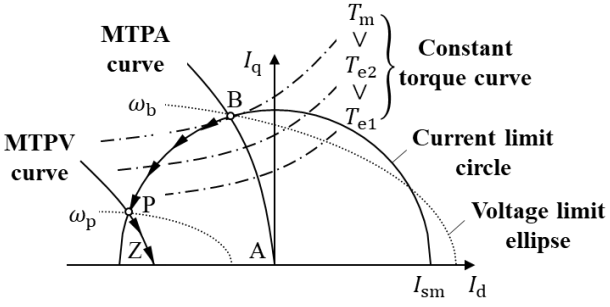

Figure 2: The Optimal Current Vector Trajectory

Presented at 47th European Rotorcraft Forum, United Kingdom, 7-9th September, 2021

First, for a given current magnitude, MTPA control operates the PMSM with an optimal phase angle that can maximize the eletromagnetic torque T_e.

(3) $T_e = \frac{3}{2}\frac{P}{2}\left[\lambda_0 I_q + (L_d - L_q) I_d I_q\right]$

Here, optimal current vector can be ontained by differentiating Eq. (3) with respect to the phase angle. For the peak torque, the optimal current vector is calculated as Eqs. (4) and (5)

(4) $I_{dm} = \frac{\lambda_0}{2(L_q - L_d)} - \sqrt{\frac{\lambda_0}{16(L_q - L_d)^2} + \frac{I_{sm}^2}{2}}$

(5) $I_{qm} = \sqrt{I_{sm}^2 - I_{dm}^2}$

That is, PMSM can be operated with MTPA control up to point B where current limit circle and voltage limit ellipse intersect, and the motor speed at point B is called base speed ω_b [Eq. (6)].

(6) $\omega_b = \frac{V_{sm}}{\sqrt{(L_d I_{dm} + \lambda_0)^2 + (L_q I_{qm})^2}}$

When the PMSM drives at a higher motor speed than ω_b, FW control is applied with the maximum terminal voltage. Under the critical condition given by the current-limit circle and voltage-limit ellipse, obtainable torque decreases from point B to P. In the FW operation, the current vector is calculated with the current-limit and voltage-limit, as Eqs. (7) and (8)

(7) $I_{dn} = -\frac{-2L_d\lambda_0 + \sqrt{(2L_d\lambda_0)^2 - 4(L_d^2 - L_q^2)\left(\lambda_0^2 + L_q^2 I_m^2 - \left(\frac{V_m}{\omega_e}\right)\right)}}{2(L_d^2 - L_q^2)}$

(8) $I_{qn} = \sqrt{I_{sm}^2 - I_{dn}^2}$

The decreased torque is obtained by substituting the calculated current vector into Eq. (3).

After the current vector reaches point P, the MTPV control allows the PMSM to produce more torque than the FW control. That is, PMSM is operated with the MTPV control for the voltage-limited maximum output power operation. Since it is difficult to calculate the direct solution of the minimum speed ω_p, ω_p is obtained as the motor speed at which T_n—torque with the FW control— and T_p— torque with the MTPV control— have the same value. T_p can be calculated using the Eq. (3) and the current vector [Eqs. (9)-(11)].

(9) $I_{dp} = -\frac{\lambda_0}{L_d} - \Delta I_d$

(10) $I_{qp} = \frac{\sqrt{(V_{sm}/\omega_e)^2 - (\Delta I_d L_d)^2}}{L_q}$

where

(11) $\Delta I_d = \frac{\frac{L_q}{L_d}\lambda_0 + \sqrt{\left(\frac{L_q}{L_d}\lambda_0\right)^2 + 8\left(\frac{L_q}{L_d} - 1\right)^2\left(\frac{V_{sm}}{\omega_e}\right)}}{4(L_d - L_q)}$

In addition, the efficiency of the motor can be calculated with the voltage and current obtained by the three control strategies.

(12) $\eta_{motor} = \frac{P_e}{P_e + P_{loss}} = \frac{P_e}{P_e + P_{Cu} + P_{Fe} + P_{no-load}}$

where copper loss P_{Cu} is calculated as $3I_{RMS}^2 R$ and iron loss P_{Fe} is the sum of the eddy current loss and hysteresis loss.

To demonstrate the capability of the proposed motor-analysis method, the example is presented in Fig. 3, which is obtained using the parameters of the Prius 2004 motor [11]. The maximum efficiency of the Prius 2004 motor appears at the region of 150 Nm torque and 2500 RPM, and the further away from this range, the lower the efficiency. That is, the proposed method can consider the change in the motor's efficiency according to the operating condion.

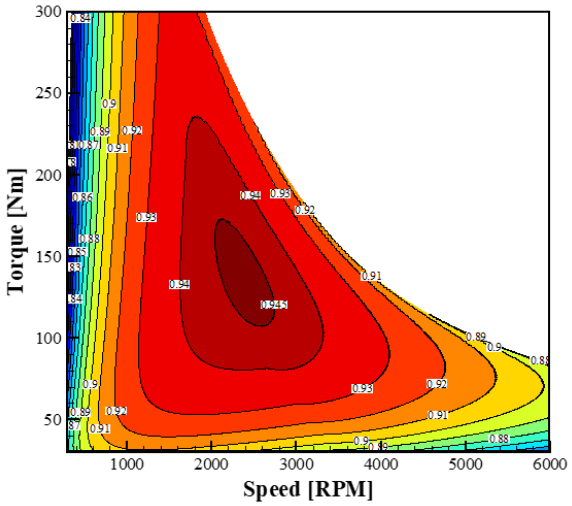

Figure 3 Example of the Efficiency Map for Prius 2004

2.2. Inverter Analysis

The inverter-analysis uses the linear loss model for the power semiconductors. This mathematical modeling considers the two types of power losses: the switching loss and conduction loss.

The switching loss of the insulated-gate bipolar transistor (IGBT) and diode is given by Ref. [13],

(13) $P_{ls} = \frac{f_s}{\pi}\left(E_{on,I} + E_{off,I} + E_{off,D}\right)\frac{V_{DC}}{V_{ref}}\frac{\sqrt{I_d^2 + I_q^2}}{I_{ref}}$

where $E_{on,I}$ and $E_{off,I}$ are the turn-on and turn-off energies of the IGBT, repectively. $E_{off,D}$ is the turn-off energy of the diode due to reverse recovery charge current. V_{ref} and I_{ref} are the reference voltage and current, respectively.

The conduction loss of the insulated-gate bipolar transistor (IGBT) and diode can be expressed as follows [14]:

Presented at 47th European Rotorcraft Forum, United Kingdom, 7-9th September, 2021

(14) $P_{\mathrm{lc,I}} = \left(\frac{1}{2\pi} + \frac{1}{8} M \cos\beta\right) V_{\mathrm{ce0}} \sqrt{I_{\mathrm{d}}^2 + I_{\mathrm{q}}^2} + \left(\frac{1}{8} + \frac{1}{3\pi} M \cos\beta\right) R_{\mathrm{ce}} \left(I_{\mathrm{d}}^2 + I_{\mathrm{q}}^2\right)$

(15) $P_{\mathrm{lc,D}} = \left(\frac{1}{2\pi} - \frac{1}{8} M \cos\beta\right) V_{F} \sqrt{I_{\mathrm{d}}^2 + I_{\mathrm{q}}^2} + \left(\frac{1}{8} + \frac{1}{3\pi} M \cos\beta\right) R_{\mathrm{F}} \left(I_{\mathrm{d}}^2 + I_{\mathrm{q}}^2\right)$

where V_{ce0} and R_{ce} are the IGBT's threshold voltage and differential resistance. V_{F}, and R_{F} are the diode's threshold voltage and differential resistance, respectively. Modulation index M can be calculated with the amplitude of the line-to-neutral inverter output voltage to one-half of the available DC bus voltage [Eq. (16)].

(16) $M = \frac{V_{\mathrm{s}}}{V_{\mathrm{DC}}/2}$

In addition, the efficiency of the inverter can be calculated considering the switching loss and the conduction loss as Eq. (17):

(17) $\eta_{\mathrm{inv}} = \frac{P_{\mathrm{motor}}}{P_{\mathrm{motor}} + P_{\mathrm{loss,inv}}} = \frac{P_{\mathrm{e}}/\eta_{\mathrm{motor}}}{P_{\mathrm{e}}/\eta_{\mathrm{motor}} - 6\left(P_{ls} + P_{lc,I} + P_{lc,D}\right)}$

where

(18) $P_{\mathrm{loss,inv}} = 6\left(P_{ls} + P_{lc,I} + P_{lc,D}\right)$

Parameters required to perform the inverter-analysis—$E_{\mathrm{on,I}}$, $E_{\mathrm{off,I}}$, $E_{\mathrm{off,D}}$, V_{ref} , I_{ref} —can be obtained from the datasheet*.

2.3. Battery Analysis

Battery analysis module is performed using a simple nearly–linear discharge model, which is a empirical model fit to a battery discharge curve as shown Fig. 4.

In the discharge model, the cell voltage could be expressed as follows [15]:

(19) $V_{\mathrm{c}}^{i} = 0.5(V_0 - KQ^i) + 0.5\sqrt{(V_{\mathrm{c0}} - KQ^i)^2 - 4(R_{\mathrm{c}}P_{\mathrm{c}} + GQ^iP_{\mathrm{c}})}$

where the battery cell power P_{c} is calculated by dividing the battery pack power P_{b} by the number of battery cells:

(20) $P_{\mathrm{c}} = \frac{P_{\mathrm{b}}}{N_{\mathrm{parallel}} \times N_{\mathrm{series}}}$

In addition, to consider the battery's voltage drop according to the depth of discharge (DOD), Q should be updated as Eq. (21) at the next time step.

(21) $Q^{i+1} = I_c^i \Delta t = \frac{P_{\mathrm{c}}}{V_{\mathrm{c}}^i} \Delta t$

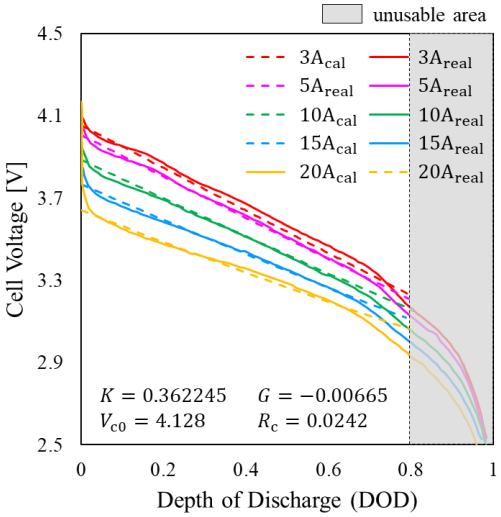

Figure 4 Example of the Battery Discharge Model For the Samsung INR 18650-30Q [15]

3. CONCEPTUAL DESIGN METHODOLOGY WITH THE PROPOSED ANAYSIS MEHOTD

To consider the characteristics of the electric propulsion system, three analysis modules—motor analysis, inverter analysis, and battery analysis—were added to the conceptual design framework presented at 45th ERF [16]. In addition, motor-sizing module is modified to obtain the parameters required for the motor-analysis module.

The overall flow of the conceptual design methodology is illustrated in Fig. 5. First, the sizing of the eVTOL aircraft is conducted to find the maximum take-off weight (MTOW), specification of the electric propulsion system required to perform the mission. The motor sizing is performed to design a rubber motor based on the maximum continuous torque T_{max}, which is obtained by comparing the shaft torque throughout the mission. Based on the T_{max} , the maximum continuous power P_{max} —equal to the product of the T_{max} and $\mathrm{RPM}_{\mathrm{max}}$—is obtained from the regression model. The other specifications required to perform the motor-analysis are derived using the regression model and P_{max}. In this paper, the regression model is constructed with the data of EMRAX motor, which was developed for the aircraft industry. Then, the mission-analysis module calculates the total capacity discharged with the four analysis modules: flight-analysis, motor-analysis, inverter-analysis, and battery-analysis. Through this process, the minimum number of battery cells is estimated to satisfy the design requirements: maximum voltage required and maximum DOD. Weight-estimation module calculates the aircraft

* Data available online at https://www.alldatasheet.com/ [retrieved 10 July 2021].

Presented at 47th European Rotorcraft Forum, United Kingdom, 7-9th September, 2021

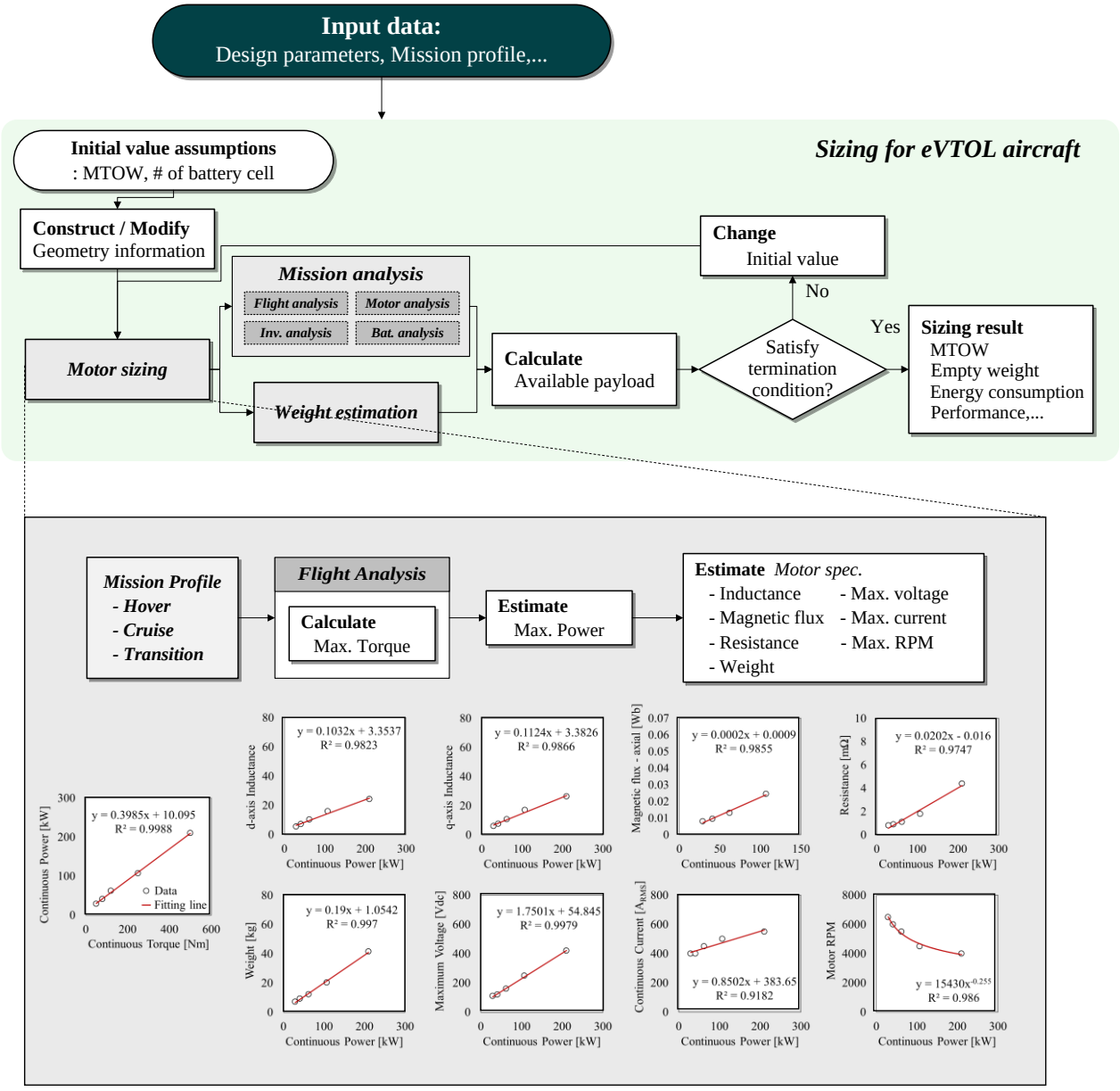

Figure 5 Overall Design Flow Chart

empty weight. Then, the available payload is calculated by subtracting the sum of empty weight and battery weight from MTOW. The difference between the available payload and required payload is used as the sizing module's termination condition. Here, the initial number of battery cell is used to consider the depth of discharge when calculating the first iteration.

4. APPLICATION OF PROPOSED METHOD

4.1. Problem Definition

To demonstrate the capability of the proposed analysis method for the electric propulsion system, VTOL aircraft sizing was performed for the Wisk Cora, a representative UAM vehicle concept. Wisk Cora can be viewed visually using the 3D modeling results in Figure 6. Its geometric data and design parameters are detailed in Appendix. For a comparative study between analysis methods under identical conditions, eVTOL aircraft sizing is performed for the same MTOW.

Presented at 47th European Rotorcraft Forum, United Kingdom, 7-9th September, 2021

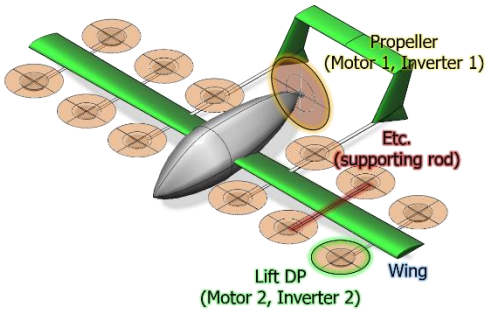

Figure 6 Three-dimensional modeling of Wisk Cora.

The mission profile used for the eVTOL aircraft sizing was a simplified Uber Elevate mission profile (Fig. 7).

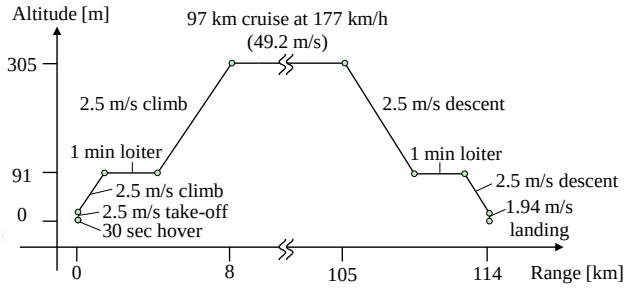

Figure 7 Simplified Uber Elevate Mission Profile [17]

4.2. Design Condition

The eVTOL aircraft sizing is performed in two cases depending on the type of analysis method for the electric propulsion system. Case 1 is a simple analysis method mainly used in previous studies [3-7, 16], and case 2 is an advanced analysis method proposed in this paper. The design conditions used for each analysis method are as follows:

Case 1: Simple analysis method

- Motor (lift DP / propeller): The efficiency coefficient as a constant, (0.88 / 0.95). The specific power is 3.65 hp/lb.
- Inverter (lift DP / propeller): the efficiency coefficient as a constant, (0.98 / 0.98). The specific power is 7.3 hp/lb.
- Battery: Energy in a box. The specific energy is 0.1825 hph/lb

Case 2: Advanced analysis method

- Motor (lift DP / propeller): Equivalent circuit analysis with three types of operation strategies for the PMSM. In addition, the regression models for the motor's specification and no-load power are used based on the EMRAX motor's database. Iron loss is assumed as 1.5 % of the mechanical power [18]. Weight is estimated using the regression model instead of using the specific power.
- Inverter (lift DP / propeller): Linear loss model for the power semiconductors. In this paper, Infineon model FF600R12ME4B72BOSA1 was used. Weight is estimated using the specific power, 7.3 hp/lb.
- Battery: Nearly–linear discharge model based on the SAMSUNG INR18650-30Q. Weight is calculated with the specific energy, 0.1825 hph/lb

4.3. eVTOL Aircraft Sizing

MTOW was set to 2130 lb calculated as the sizing result of case 1, and sizing of case 2 was performed with the fixed MTOW, 2130 lb. The sizing results are summarized in Table 1.

Table 1: Results of the eVTOL Aircraft Sizing

Weight	Case 1	Case 2
Empty weight [lb]	1,790	2,106
Structure group weight [lb]	638	637
Battery [lb]	378	393
$(N_{\text{cell,series}}, N_{\text{cell,parallel}})$	(- / -)	(141 / 35)
Electric motor [lb]	148	373
Inverter [lb]	75	121
Etc. (Wiring, System,…) [lb]	551	582
Available payload [lb]	400	84

In case 2 using the advanced analysis method, the weight of the electric propulsion system was predicted to be greater than in case 1 using the simple analysis method. First, the battery weight was predicted to be larger from 378 lb to 393 lb, which means that the efficiency of the motor and inverter in case 2 was lower than in case 1. Figure 8 is a graph of the efficiency of the motor and inverter for each mission element, where the bar and line indicate the efficiency of each electric device and the efficiency of the electric propulsion system, respectively. First, the motors' efficiencies of case 2 are approximately 0.95, except for the descent mission segment. It means that most of the operation points of the sized motors are in the optimal region when performing a given mission. In descending flight, the motor efficiency was relatively reduced to 0.93 since the torque applied to the motor was too small (Fig. 9).

Presented at 47th European Rotorcraft Forum, United Kingdom, 7-9th September, 2021

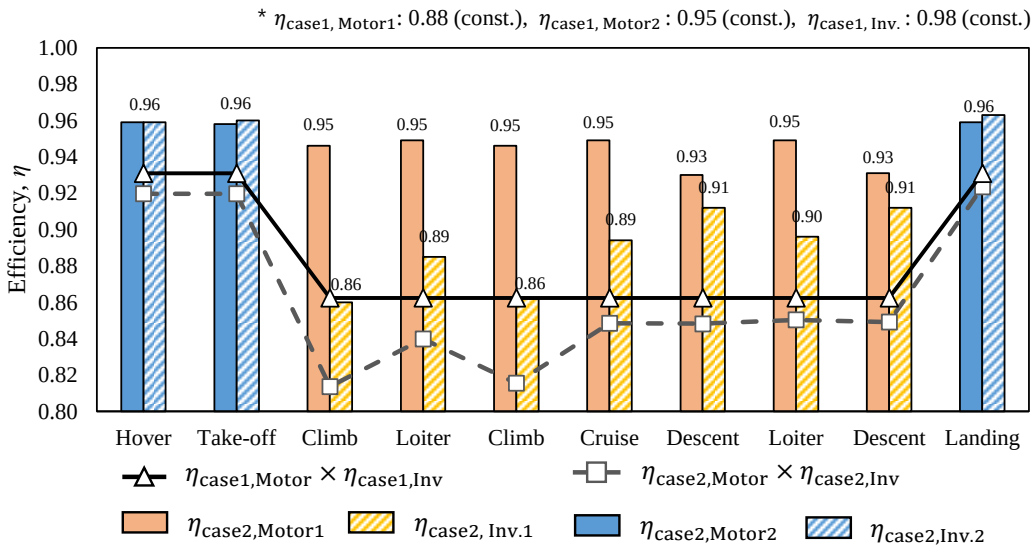

Figure 8 Efficiency of Electric devices for the Mission Profile

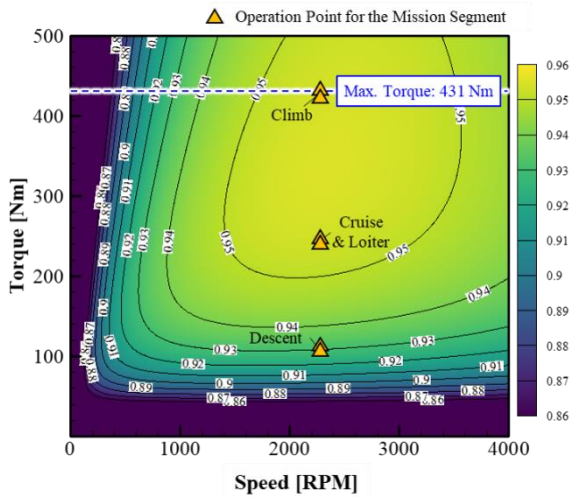

a

(a) Motor 1 (Lift DP)

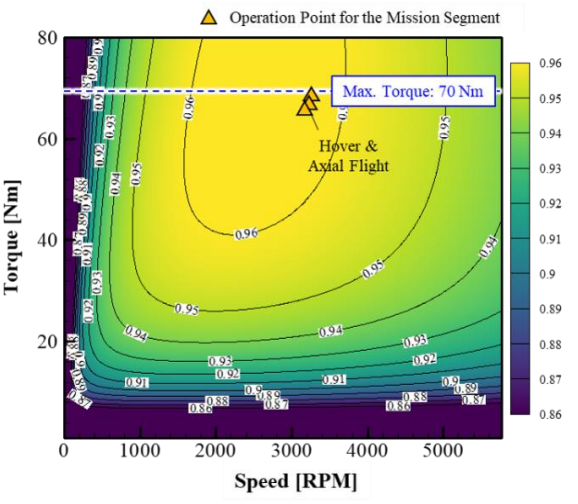

(b) Motor 2 (Thruster for cruise)

Figure 9 Efficiency Map for the Sized PMSMSs

In addition, the higher the output voltage and current of the inverter are required, the greater the switching loss and conduction loss of the inverter occur. Inverter 1 for the single propeller requires a much higher output current and voltage than an inverter 2 used in multiple motors for lift DP. Therefore, the efficiency of inverter 1 has a relatively lower value of 0.86 to 0.91.

The motor efficiency of case 2 was higher than that of case 1, but the inverter efficiency showed the opposite result. Considering both of these results, the efficiency of the electric propulsion system was lower in case 2 than in case 1 throughout the mission profile, which resulted in the increase in battery weight.

The weight for the motor and inverter in case 2 was predicted to be higher for the following reasons. Case 1 estimates the weight using only maximum continuous power and specific power without considering the motor's maximum continuous torque and maximum RPM: $W_{motor} = \frac{P_{max,motor}}{SP}$. Since the regression model used in case 2 considers the maximum continuous torque and maximum RPM, which are actual motor‘s specification, conservative results are obtained. Since the inverter is also sized based on the maximum continuous power that reflects the maximum continuous torque and maximum RPM, the inverter of case 2 is sized larger than that of case 1. For these reason, the weight of the electric propulsion system in case 2 is predicted to be larger than in case 1.

The battery analysis results for each mission segment are shown in Figure 10. First, the greater the shaft power is required for mission performance, the greater the current of the battery and the lower the voltage occurs. Furthermore, the voltage drop is visible in the cruise mission that takes the most time.

Presented at 47th European Rotorcraft Forum, United Kingdom, 7-9th September, 2021

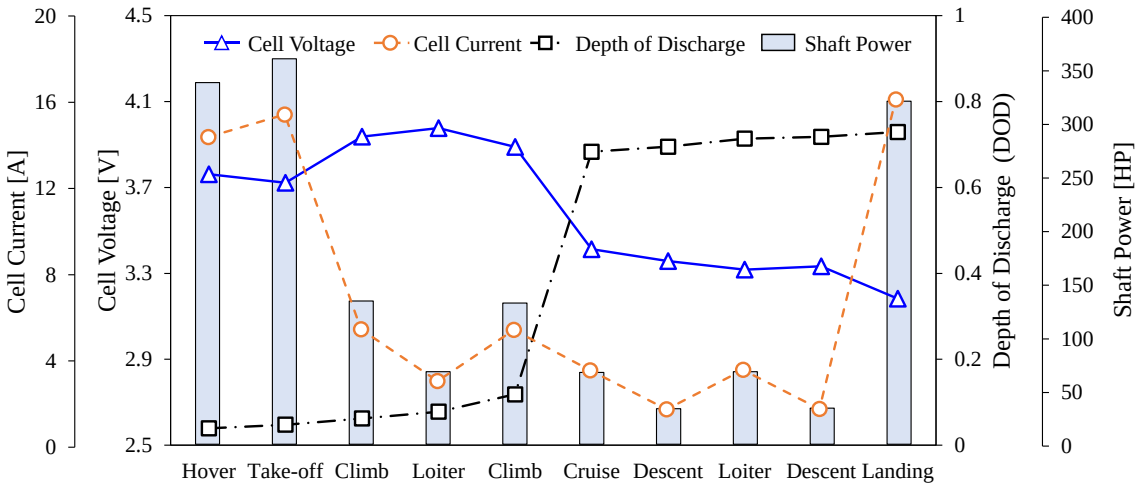

Figure 10 Battery Analysis Results for Each Mission Segment

Due to the voltage drop, the result was derived that the cell current at the landing mission was more significant than the cell current at the hovering, although the required shaft power at the landing was smaller than the shaft power at the hovering.

Based on the characteristics of the existing electric propulsion system, the eVTOL aircraft was sized, and the available payload was reduced by 40 lb compared to the existing simple analysis method.

5. CONCLUSION

In this study, an advanced analysis method of the electric propulsion system for UAM vehicles was proposed. To this end, three models were primarily presented: motor-analysis, inverter-analysis, and battery-analysis module. These modules can hanlde the electric characteristics of the electric devices. First, a motor-analysis module was developed to handle PMSM's control strategies—MTPA, FW, and MTPV. Second, the inverter-analysis module was constructed considering the switching loss and conduction loss. Moreover, based on the near-linear discharge model, the battery-analysis module was constructed to consider the voltage drop. In order to demonstrate the capability of the proposed analysis method for the electric propulsion system, the eVTOL aircraft sizing was performed in two cases depending on the type of analysis method for the electric propulsion system. Through the comparative study, the conclusions were as follows:

1) PMSM can have a very high efficiency of 96% when operated in an operation region. In addition, when a single PMSM is used instead of multiple PMSM, the high voltage and current required by the PMSM can occur a huge switching loss and conduction loss of the inverter.
2) The motor should be sized based on the maximum continuous power determined by the maximum torque and maximum rotation speed.
3) The voltage drop caused by the increase in DoD increases the cell current, which accelerates battery consumption.

These results can provide insight into the characteristics of the electric propulsion system. The general regression models for inverters and batteries as well as motors should be considered as additional improvements. Also, an design of the thermal management system through the thermal analysis is needed for the electric propulsion system to make the design even more realistic.

ACKNOWLEDGEMENT

This research was supported by Unmanned Vehicles Core Technology Research and Development Program through the National Research Foundation of Korea(NRF) and Unmanned Vehicle Advanced Research Center(UVARC) funded by the Ministry of Science and ICT, the Republic of Korea (2020M3C1C1A02081911)

REFERENCE

[1] Electric VTOL News by the Vertical Flight Society, “eVTOL Aircraft Directory,” retrieved 01 August 2020. https://evtol.news/aircraft/

[2] de Vries, R., Brown, M., and Vos, R., “Preliminary Sizing Method for Hybrid-Electric Distributed-Propulsion Aircraft,” Journal of Aircraft, Vol. 56, No. 6, 2019, pp. 2172–2188.

[3] de Vries, R. D., Hoogreef, M. F. M., and Vos, R., “Range Equation for Hybrid-Electric Aircraft with Constant Power Split,” Journal of Aircraft, Vol. 57, No. 3, 2020, pp. 552–557.

[4] de Vries, R. D., Hoogreef, M. F. M., and Vos, R., “Aeropropulsive Efficiency Requirements for

Presented at 47th European Rotorcraft Forum, United Kingdom, 7-9th September, 2021

Turboelectric Transport Aircraft," AIAA Scitech 2020 Forum, AIAA Paper 2020-0502, 2020.

[5] Finger, D. F., Bil, C., and Braun, C., "Initial Sizing Methodology for Hybrid-Electric General Aviation Aircraft," Journal of Aircraft, Vol. 57, No. 2, 2020, pp. 245–255.

[6] Finger, D. F., Braun, C., and Bil, C., "Impact of Engine Failure Constraints on the Initial Sizing of Hybrid-Electric GA Aircraft," AIAA Scitech 2019 Forum, AIAA Paper 2019-1812, 2019.

[7] Finger, D. F., Goetten, F., Braun, C., and Bil, C., "Initial Sizing for a Family of Hybrid-Electric VTOL General Aviation Aircraft," 67. Deutscher Luft- und Raumfahrtkongress DLRK2018, DGLR, Bonn, Germany, 2018, Paper 0102.

[8] Lukaczyk, T. W., Wendorff, A. D., Colonno, M., Economon, T. D., Alonso, J. J., Orra, T. H., and Ilario da Silva, C., "SUAVE: An Open-Source Environment for Multi-Fidelity Conceptual Vehicle Design," 16th AIAA/ISSMO Multidisciplinary Analysis and Optimization Conference, AIAA Paper 2015-3087, 2015.

[9] Malpica, C., and Withrow-Maser, S., "Handling Qualities Analysis of Blade Pitch and Rotor Speed Controlled eVTOL Quadrotor Concepts for Urban Air Mobility," VFS International Powered Lift Conference 2020, San Jose, CA, January 21–23, 2020

[10] Liu Q., "Analysis, design and control of permanent magnet synchronous motors for wide-speed operation," Ph.D. Dissertation, National University of Singapore, 2005.

[11] Staunton, R. H., Ayers, C. W., Chiasson, J. N., Burress, T. A., and Marlino, L. D., "Evaluation of 2004 Toyota Prius Hybrid Electric Drive System," 2006.

[12] Ding, X., Guo, H., Xiong, R., Chen, F., Zhang, D., and Gerada, C., "A new strategy of efficiency enhancement for traction systems in electric vehicles," Applied Energy, Vol. 205, 2017, pp. 880–891.

[13] Hassan W., Wang B., "Efficiency optimization of PMSM based drive system," Proceedings of the 7th International Power Electronics and Motion Control Conference, Vol. 2, Jun. 2012, pp. 1027-1033.

[14] Mestha LK, Evans PD. "Analysis of on-state losses in PWM inverters. Electric Power Applications," IEE Proceedings B, Vol. 136, No.4, 1989, pp.189–195.

[15] Misra, A. "Summary of 2017 NASA Workshop on Assessment of Advanced Battery Technologies for Aerospace Applications," NASA Glenn Research Center Report GRC-E-DAA-TN51429, Document ID: 20180001539, Cleveland, Ohio, Jan. 2018, pp. 1–18.

[16] Lee, D., Kang, S., and Yee, K., "A Comparison Study of Rotorcraft with Hybrid Electric Propulsion System," Proceedings of the 45th European Rotorcraft Forum, Warsaw, Poland, Sep. 17–20, 2018.

[17] Vegh, J. M., Botero, E., Clarke, M., Trent, J., and Alonso, J., "Current Capabilities and Challenges of NDARC and SUAVE for eVTOL Aircraft Design and Analysis," AIAA Propulsion and Energy 2019 Forum, AIAA Paper 2019-4505, Aug. 2019.

[18] Regas, B.I., "Analysis of different powertrain configurations for a formula style electric racecar," M.S. Dissertation, Universitat Politècnica de Catalunya, 2019.

[19] Bacchini, A., and Cestino, E., "Electric VTOL Configurations Comparison," Aerospace, Vol. 6, No. 3, 2016, pp. 26.

APPENDIX

Geometry data

Table A1: Geometry data

Geometry data	
Lift DP [17]	Radius: 2.0 ft Solidity: 0.2 Taper: 0.75 Collective pitch: 0.236 rad Airfoil: NACA0012 Material: aluminum 6061-T6 Parasitic drag (D/q): 1.18 ft^2 Technical factor: 0.65
Wing [17, 19]	Area: 114 ft^2 Aspect ratio: 11.4 Taper: 1.0 Incidence angle: 0.216 rad Airfoil: NACA0018 Material: aluminum 6061-T6 Technical factor: 0.65
Propeller [17]	Radius: 3.5 ft Solidity: 0.1 Airfoil: NACA0012 Material: aluminum 6061-T6 Technical factor: 0.65
Horizontal stabilizer [17]	Area: 19.1 ft^2 Aspect ratio: 4.78 Taper: 1.0 Airfoil: NACA0012 Technical factor: 0.76
Vertical stabilizer [17]	Area: 12.69 ft^2 Aspect ratio: 1.41 Taper: 0.5 Airfoil: NACA0012 Parasitic drag (D/q): 0.203 ft^2 Technical factor: 0.76
Supporting rod [17]	Material: aluminum 2024 Parasitic drag (D/q): 0.98 ft^2

Presented at 47th European Rotorcraft Forum, United Kingdom, 7-9th September, 2021

Fuselage [17]	Material: Composite Parasitic drag (D/q): 0.62 ft^2 Technical factor: 0.76
Landing gear [17]	Parasitic drag (D/q): 0.377 ft^2

Presented at 47th European Rotorcraft Forum, United Kingdom, 7-9th September, 2021